ELSEVIER

Thermochimica Acta 364 (2000) 1–10

thermochimica acta

www.elsevier.com/locate/tca

n-Dodecane melting studied by the combined use of different calorimetric modes

C. Cardelli, G. Salvetti, E. Tombari*

IFAM/CNR, Area della Ricerca, San Cataldo, via Alfieri 1, 56010 Ghezzano, Pisa, Italy

Received 16 May 2000; received in revised form 14 August 2000; accepted 20 August 2000

Abstract

The solid–liquid phase transition of *n*-dodecane has been studied with a modulated adiabatic scanning calorimeter (MASC). The well-known features of melting — such as the existence of a pre-melting region and the dependence of the melting curve on the scanning rate — were observed, together with completely new features which, to the best of our knowledge, have never been reported before, such as the presence of a small secondary, non-reproducible peak in the melting curve. This last result was obtained working in the scanning operation mode, at rates lower than 3.3×10^{-4} K s^{-1}. The complex melting process occurring in the sample was studied inside the melting temperature interval, using the temperature step scanning and the adiabatic-like enthalpy step operation mode of MASC. A very slow rate of attainment of equilibrium was observed when the liquid and solid phases were co-existing. Temperature modulation, in both the continuous scanning mode and the quasi-isothermal step-scanning mode, was also used to obtain a clearer characterisation of the melting kinetics. The melting transition of *n*-dodecane is discussed in the light of the results obtained by applying to one and the same sample different operation modes. The transition enthalpy values measured are compared to the data in the literature. The two peaks observed in the melting curve of *n*-dodecane are analysed and possible explanations for the second peak are discussed.

Keywords: *n*-Dodecane; *n*-Alkane; Modulated adiabatic scanning calorimeter; Phase transition

1. Introduction

Ideal thermodynamic conditions in the melting and crystallisation of molecular compounds are only rarely achieved due to the presence of structural relaxation processes and precursor effects caused by the non-equilibrium conformations explored by the sample [1]. The complexity of the phenomena occurring at the phase transition increases with the size of the molecule, and the temperature interval involved is generally quite large. This is particularly evident in case of the phase transitions of polymers, which are currently being widely used to test theoretical models [2,3]. The melting and crystallisation of the *n*-alkanes have also been the subject of intensive study due to very interesting features related to their polymorphism [4,5]. Calorimetric data point to the existence of rotator phases and surface crystallisation, at least in those *n*-alkanes with more than 20 carbon atoms [6–8].

The aim of the present study was to gather data on these processes by means of a modulated adiabatic scanning calorimeter (MASC) recently built by the authors [7]. MASC operates in three different modes: (i) scanning the sample temperature; (ii) modulating

* Corresponding author. Tel.: +39-50-3152536; fax: +39-50-3152230.
E-mail address: tombari@ifam.pi.cnr.it (E. Tombari).

0040-6031/00/$ – see front matter
PII: S0040-6031(00)00642-0

the temperature at a fixed frequency and amplitude; and (iii) maintaining adiabatic-like conditions. For these preliminary experiments (before attempting to study the polymorphism of polyolefins and *n*-alkanes with longer molecular chains), *n*-dodecane was chosen as the reference *n*-alkane, and all measurements were performed on a single sample.

MASC was first used in the temperature scanning mode to obtain the apparent specific heat (C_{app}) of the sample during melting. Successively, temperature modulation was introduced in order to measure simultaneously the C_{app} and the complex heat capacity, $C'(\omega) - iC''(\omega)$, of the sample.

To study the time evolution of the process taking place in the sample, the temperature was step-scanned within the melting interval by supplying equal energy pulses under adiabatic-like conditions and extending the duration of the isothermal part of each step, in order to observe the structural relaxation and re-crystallisation processes of the polycrystalline solid–liquid mixture [1,9].

The calorimetric data thus obtained on *n*-dodecane provide considerable insight into the complexity of the melting processes in polycrystalline samples and underline the intrinsic difficulty of their characterisation in systems with transitions that are remote from the ideal thermodynamic behaviour. The main features of the experimental curves, such as the presence of a second peak for the melting region, are discussed and the fusion enthalpy values obtained are compared with the data in the literature.

2. Experimental

MASC is a single cell calorimeter, which has been described in detail elsewhere [7,10]. The sample consisted of *n*-dodecane (>99.8% purity) purchased from Fluka Chemical Co. and used without additional purification. The sample container was a cylindrical Pyrex tube (o.d. = 3 mm; i.d. = 2.2 mm; L = 90 mm), which was partially filled with 182.60 mg of *n*-dodecane and then flame-sealed. The three operational modes of MASC, built into the instrument's software, were used in successive runs on this sample.

The procedure used to obtain the solid phase in the calorimetric cell was the following: the melt was heated to −5°C, then cooled at a rate of 3 K s^{-1} and, after freezing, stored at −20°C for 1 h. The sample thus obtained was studied over three runs at a heating rate of 1/6000 K s^{-1}. A good repeatability of the area of the melting peak was obtained, although a few features of the melting profile were not always reproduced. The cell temperature and the power supplied to the cell were measured at time intervals of 2 s and the values were recorded. The quantities of interest were calculated using the equations described in reference [11]. The temperature was measured with an accuracy of 0.01 K, while the instrument is capable of measuring temperature differences as small as 0.0001 K. The accuracy of the heat flow rate was 100 μW and the minimum detectable power was 20 μW.

3. Experimental results

The temperature dependence of the apparent heat capacity, C_{app}, calculated from the measured heat flow rate at different temperature scanning rates, is shown in Fig. 1. The experimental curves changed in shape and the melting peaks shifted towards the lower temperature values with the decreasing rate of the temperature scan, β. The same behaviour has been observed in standard DSC measurements, although these are generally obtained at much higher scanning rates. The C_{app} curve at $\beta = 10^{-5}$ K s^{-1} has a width of approximately 0.4 K, while at $\beta = 1.25 \times 10^{-2}$ K s^{-1}, the width is >2 K. The C_{app} curves at $\beta < 5 \times 10^{-4}$ K s^{-1} sometimes display a shoulder after the peak.

The values for the melting enthalpy, ΔH_m, reported in Table 1 were obtained by integrating the C_{app} (T) curve over the entire temperature range after subtracting the baseline value as reported in Fig. 2. The baseline, which represents the heat capacity of the co-existing liquid and solid phases, was calculated from an equation fitting the heat capacity values measured below and above the melting temperature interval. The errors in Table 1 were calculated by multiplying the minimum detectable power (20 μW) by the integration time and summing the baseline uncertainty.

The average of the ΔH_m values calculated from the data obtained at $\beta > 1.66 \times 10^{-4}$ K s^{-1} is close to the value reported in the literature, 214.76 J g^{-1} [12]. The

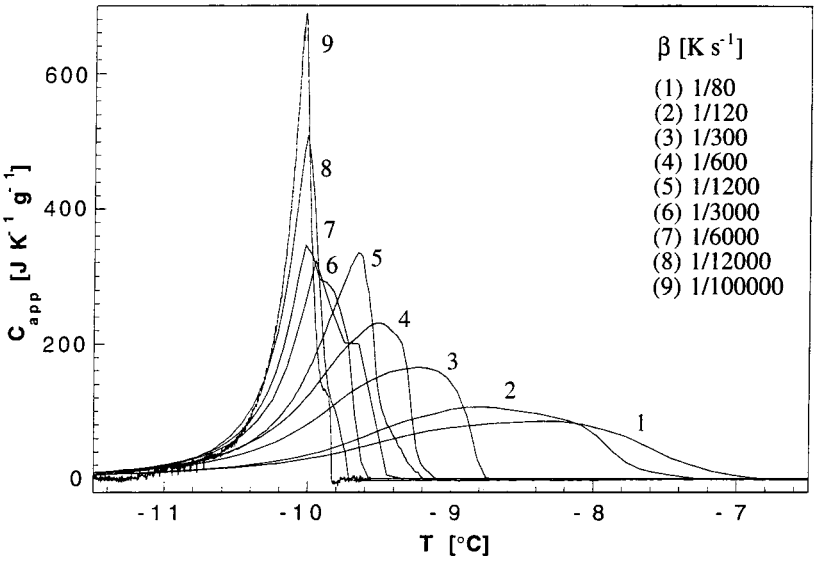

Fig. 1. The apparent specific heat of *n*-dodecane plotted against temperature at different heating rates.

integration of the curves at $\beta = 1.66 \times 10^{-4}$ K s^{-1} yielded lower values due to limits in the sensitivity of the instrument, which was not sufficient to measure the contribution of an increasing part of the pre-melting curve.

Fig. 2 shows a typical melting peak with the most significant parameters studied. The melting temperature, T_{onset}, was calculated as the intersection of the extrapolated baseline from the solid phase region and the tangent at the flex point of the low temperature side of the curve C_{app} (T). The points of the curve in Fig. 3 represent the temperatures, calculated from the curves in Fig. 1, at which the end of melting, the peak of the melting curve, and the melting onset occur (T_{eom}, T_{peak} and T_{onset}, respectively, as defined in Fig. 2). The β-dependence of T_{eom} and T_{peak} was significant and non-linear over the explored β range: at low β values a sharp increase was evident in the two curves. At $\beta > 1/1200$ K s^{-1}, the slope of the straight line fitting the T_{eom} values was twice the slope of the line fitting the T_{peak} values, as was to be expected due to the signal deformation caused by the scanning rate. On the contrary, the β-dependence of T_{onset} was negligible, even at low β values.

Table 1
Melting enthalpy for *n*-dodecane measured at different temperature scanning rates

β (K s^{-1})	ΔH_m (J g^{-1})
12.5×10^{-3}	212.9 ± 1.2
8.33×10^{-3}	213.1 ± 1.2
3.33×10^{-3}	212.1 ± 1.4
1.66×10^{-3}	211.5 ± 1.8
8.33×10^{-4}	211.0 ± 2.4
3.33×10^{-4}	214.0 ± 4.0
1.66×10^{-4}	213.0 ± 8.0
8.33×10^{-5}	201.0 ± 15.0
1.00×10^{-5}	180.0 ± 50.0

Fig. 4 shows the behaviour of C_{app} and of the real, $C'(\omega)$, and imaginary, $C''(\omega)$, components of the complex heat capacity, calculated from a modulated temperature scanning run at: $\omega = 0.021$ rad s^{-1} (modulation period $\tau = 300$ s); modulation amplitude $\delta T = 0.025$ K; and $\beta = 1/6000$ K s^{-1}. Under these experimental conditions, the response of the sample+cell system was linear within the melting region, as may be deduced from the absence of any signal at 2ω and 3ω.

The melting and re-crystallisation processes provoked by the small temperature modulation amplitude are reflected in the $C'(\omega)$ and $C''(\omega)$ curves. In

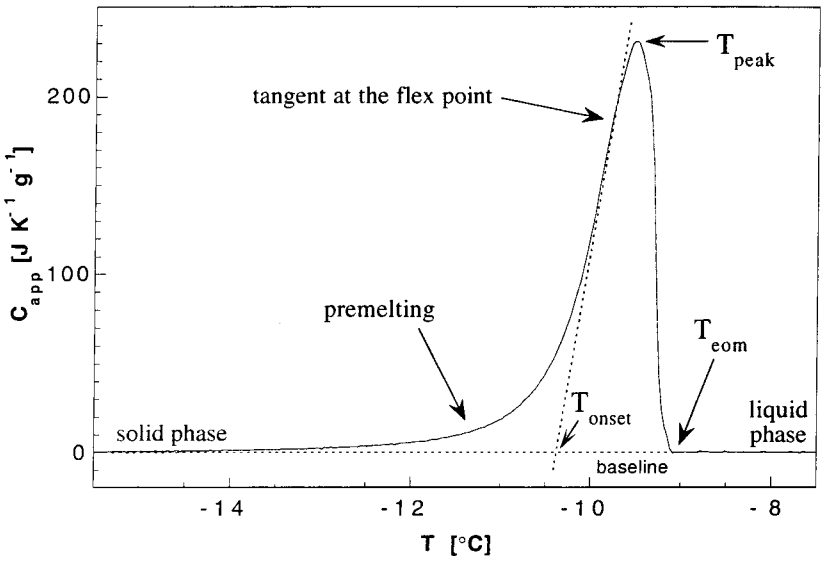

Fig. 2. The apparent specific heat of *n*-dodecane plotted against temperature at $\beta = 1/600$ K s^{-1}. The melting peak analysis which was used to determine the "end of melting" temperature (T_{eom}), the peak temperature (T_{peak}), and the onset temperature (T_{onset}) is also shown.

particular, $C'(\omega)$ is nearly coincident with C_{app} and $C''(\omega)$ is nearly null at $T < -11.5$°C. At higher temperatures, $C''(\omega)$ rises and $C'(\omega)$ becomes more and more different from C_{app}, decreasing to the value of the heat capacity of the liquid just before the end of the melting.

The adiabatic-like operation mode was used to carry out a time-domain analysis within the melting

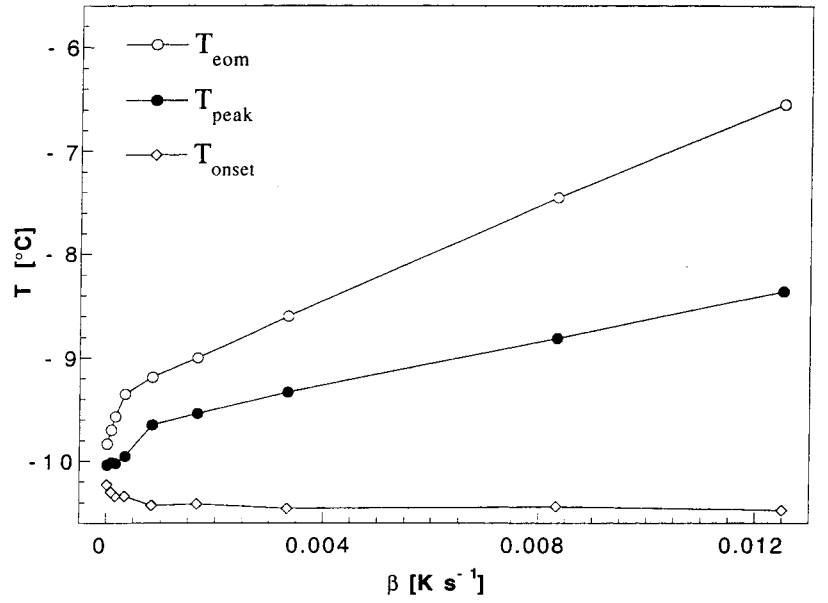

Fig. 3. T_{eom}, T_{peak}, and T_{onset} plotted against the scanning rate, calculated from the curves in Fig. 1 following the procedure outlined in Fig. 2.

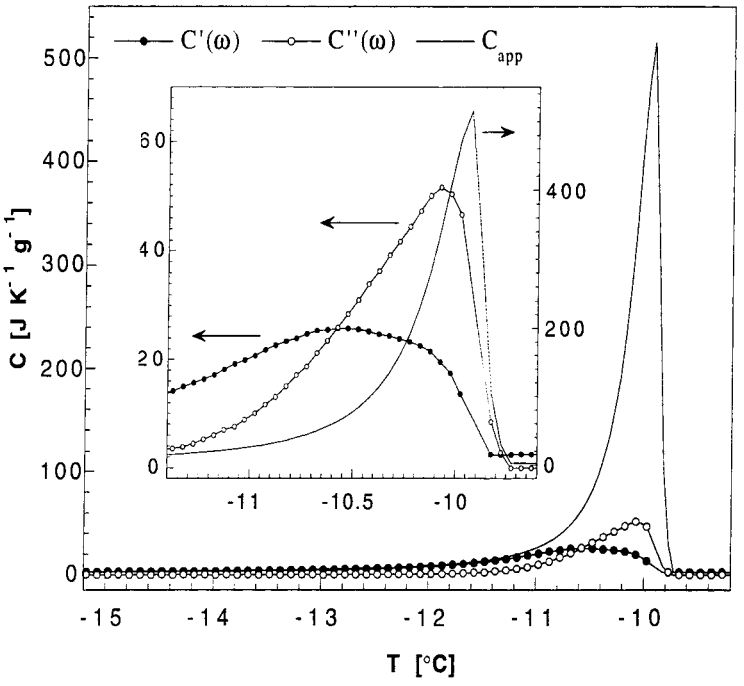

Fig. 4. The real and imaginary components of the complex heat capacity and the apparent specific heat plotted against the temperature measured at $\beta = 1/6000$ K s^{-1}, $\delta T = 0.025$ K, and $\tau = 300$ s.

interval. The results are summarised in Fig. 5, which shows the cell temperature measured during successive, equal heat pulses of 2.40 J supplied for a 50 s period at time intervals of 400 s. The temperature range explored included the pre-melting interval, the melting interval, and the liquid phase. The melting interval was then explored by applying energy pulses (0.24 J for 50 s) to the cell at time intervals of 400 s. The $T(t)$ curve is shown in Fig. 6. The data reported in Figs. 5 and 6 underline the fact that intervals of 400 s are not sufficient to attain equilibrium during the final part of the melting interval, when the process becomes slower.

The characteristic heat diffusion time within the sample cell was very short ($\tau_i \sim 1$ s) in the liquid phase region, as may be seen from the Q-steps (see inset A of Fig. 6). In the melting region, the evolution over time of the cell temperature after the heat pulse followed the energy absorption process as a consequence of the heat diffusion, phase transformation and structural relaxation of the sample (see inset B of Fig. 6).

Finally, the temperature step-scanning mode was used to study the kinetic processes taking place in the sample. In Fig. 7, the behaviour of the heat flow rate, $P(t)$, is shown. $P(t)$ was measured during a run where the temperature was scanned between -11.8 and -9.4°C with steps of 0.2°C followed by isotherms of 1800 s. The liquid fraction, x_{liq}, calculated from the integral of $P(t)$ normalised to the total ΔH_m, is also shown in Fig. 7. When equilibrium between the co-existing phases was attained (as was the case in this run except during one step), the final values for x_{liq} at the end of each isotherm describe the solid–liquid co-existence curve of *n*-dodecane in the melting interval.

The $P(t)$ curves obtained from a temperature step-scan performed between -10.4 and -9.9°C (equal steps of 0.05°C followed by isotherms of 6000 s) are displayed in Fig. 8. One curve was obtained with superimposed temperature modulation ($\tau = 300$ s; $\delta T = 0.025$°C). Each data point in the figure represents the average of $P(t)$ over a modulation period; in the case of the non-modulated run each point

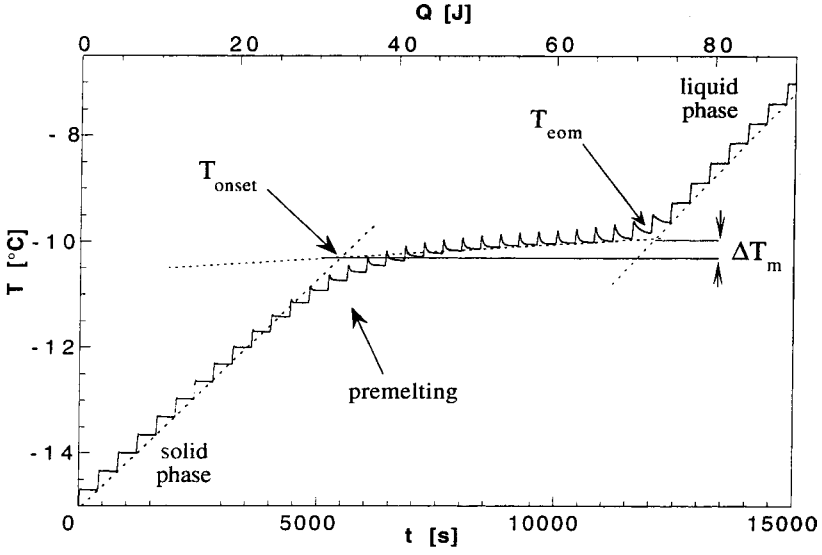

Fig. 5. The cell temperature plotted against time (and against the amount of energy supplied to the cell) measured in the adiabatic-like step-scanning mode (heat pulses: 2.4 J supplied for 50 s at time intervals of 400 s). The method used to calculate T_{onset} and the melting interval ΔT_m is also shown.

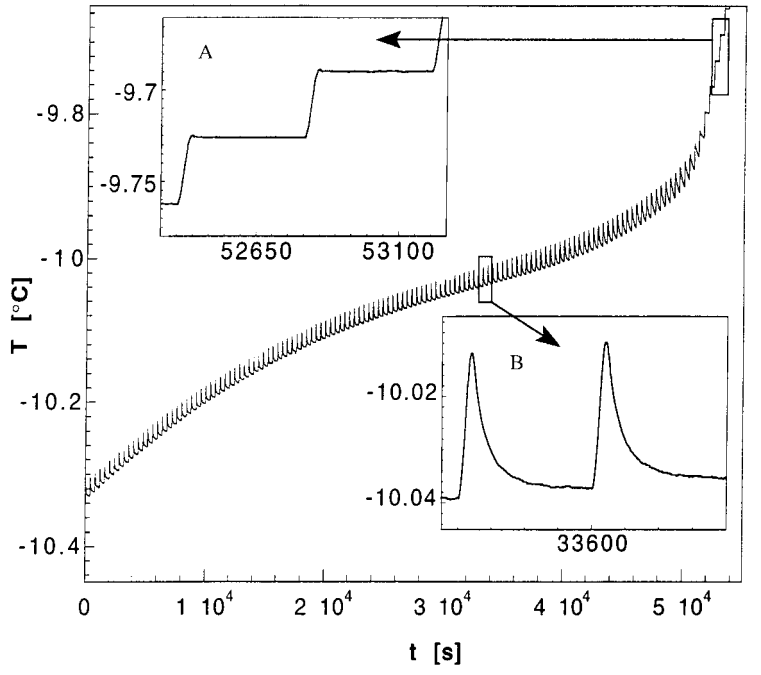

Fig. 6. Cell temperature plotted against time, measured using the adiabatic-like step-scanning mode (heat pulses: 0.24 J supplied for 50 s at time intervals of 400 s).

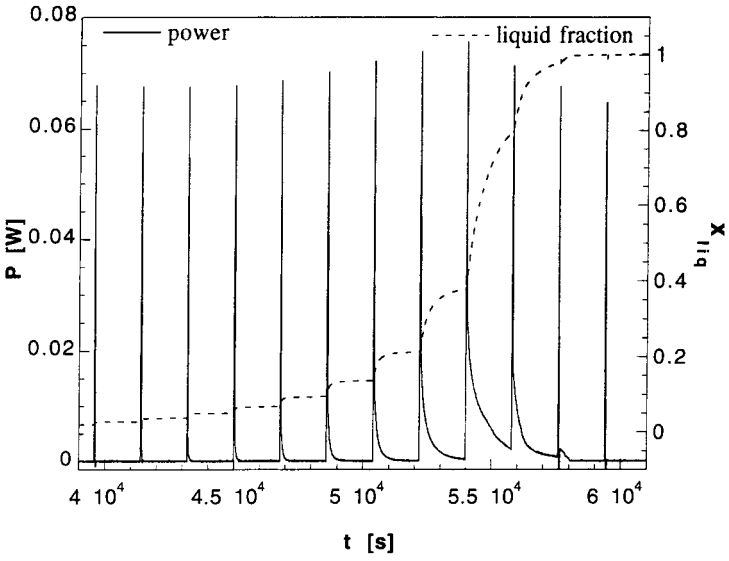

Fig. 7. The power supplied to the cell and the sample liquid fraction, calculated from the power integral curve, plotted against time during a step-scanning run (*T*-step: 0.2 K; step-length 1800 s). The scanned temperature interval was −11.8 to −9.4°C.

represents the mean value of 10 readings at time intervals of 2 s. The two curves display practically the same profile. The values for $C'(\omega)$ and $C''(\omega)$, calculated from the modulated run using the procedure described in [11], are shown in Fig. 9. The $C'(\omega)$ and $C''(\omega)$ curves are in agreement with the curves in Fig. 4 for the corresponding temperature interval. They contain further information on the reversibility and kinetics of the processes by which the sample attains equilibrium.

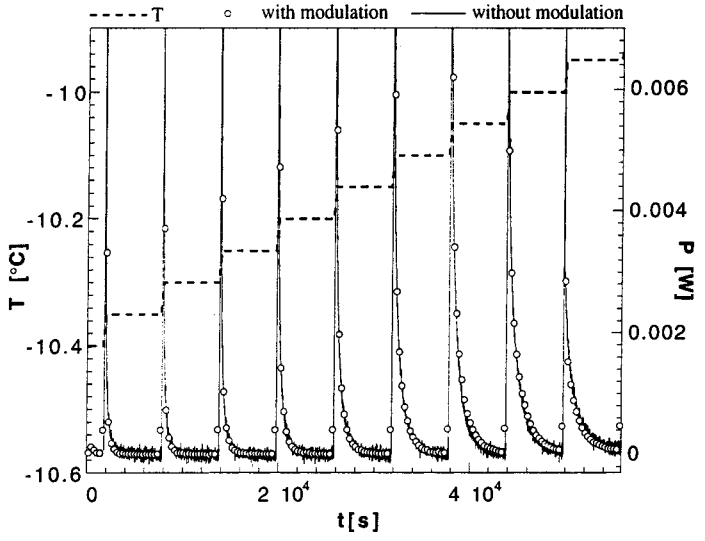

Fig. 8. The cell temperature and power supplied to the cell plotted against time during a step-scanning run (*T*-step: 0.05 K, step-length 6000 s) with and without modulation at $\omega = 0.021$ rad s^{-1} ($\tau = 300$ s) and $\delta T = 0.025$ K.

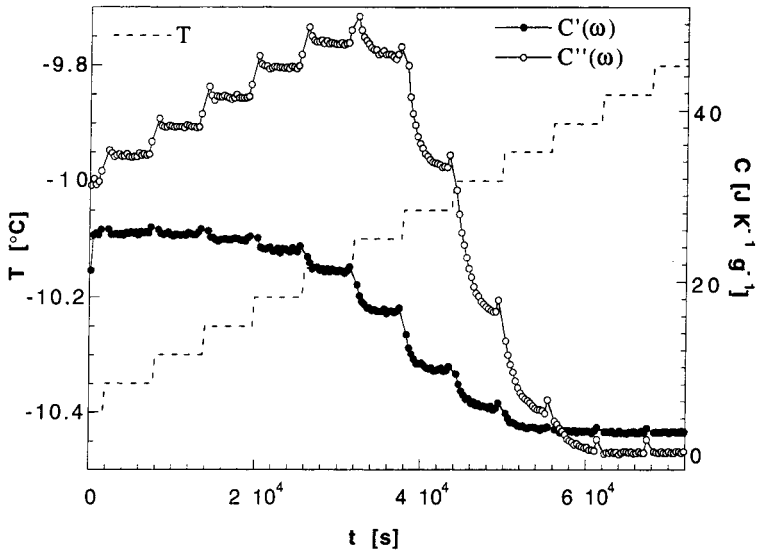

Fig. 9. The cell temperature, $C'(\omega)$ and $C''(\omega)$ plotted against time, as calculated from the experimental curves in Fig. 8.

4. Discussion

This experimental study underlines the difficulty of determining a temperature value associated with the melting transition, since the melting curve is so strongly dependent on the scanning rate. Indeed the main peak shifts towards higher temperatures by an amount $\beta\tau_i$, where τ_i is the sum of the heat diffusion time from the cell heater to the sample's solid fraction + the characteristic time of the melting process. Moreover, the melting peak width decreases with the scanning rate towards a limit value which is influenced by the sample's purity and polycrystallinity. Indeed, the melting temperature of any crystallite changes with its size, shape and defect/impurity content; moreover, crystallites can perfect through local melting and re-crystallisation processes [9].

The standard thermodynamic definition of the melting temperature is based on the existence of a plateau in the T versus sample enthalpy curve. No such plateau was observed for *n*-dodecane, as can be seen in Figs. 5 and 6, but it was possible to define a temperature interval, ΔT_m, in which the melting occurs.

The pre-melting region extends for many degrees below -10.40°C and is detectable down to -15°C (see Figs. 2 and 4). As Fig. 3 shows, T_{onset}, calculated using a procedure equivalent to that used to determine the melting temperature in standard DSC [13], is practically independent of the scanning rate. Its value, -10.35 ± 0.03°C, is in good agreement with the initial temperature value for the melting interval, ΔT_m (compare the adiabatic-like run in Fig. 5). Moreover, the value for ΔT_m in Fig. 5 ($\Delta T_m = 0.36$°C) is very close to the melting curve width ($T_{eom} - T_{onset} = 0.38$°C) for the run at $\beta = 10^{-5}$ K s^{-1} in Fig. 1.

These data support the use of T_{onset} to represent the melting transition, but the complexity of this transition definitely requires a more detailed description and the use of other parameters such as ΔT_m, T_{eom} and T_{peak} for its characterisation.

The curves obtained using the modulated temperature scanning mode can be analysed in terms of the following three different regions (see Fig. 4).

1. The region below -11.5°C, where $C_{app} = C'(\omega)$ and $C''(\omega) = 0$, demonstrates the reversibility of the processes contributing to C_{app} since the response time is very short compared to the modulation period. This interval can be defined as the *pre-melting region* which has as its lower limit the temperature at which C_{app} attains the solid phase C_p value.

2. The melting interval $-11.5 < T < -9.75$°C, where $C_{app} \neq C'(\omega)$, $C''(\omega) \neq 0$, and C_{app} is much greater than C' and C'', shows that the heat diffusion time within the cell (which depends upon (a) the heat transfer from the heater to the sample; and (b) the heat diffusion in the co-existing phases which supplies the latent heat of the transition) increases more and more, such that the cell + sample system is unable to follow the T modulation. Indeed, $C''(\omega)$ increases with T as $C'(\omega)$ decreases. This is supported by the observed increase in the relaxation time during the step-scanning measurements (see Figs. 5–8). We are currently developing a theoretical model that will link these time domain and frequency domain results with the heat diffusion and process kinetics of a given system.
3. The region above -9.75°C, where $C'(\omega) = 0$ and $C_{app} = C'(\omega)$. Here, the melting of the sample is complete and $C'(\omega) = C_p = 2.37\ J\ K^{-1}\ g^{-1}$ is the specific heat of liquid *n*-dodecane, a value which is in good agreement with the one reported in [13,14].

The average $P(t)$ measured in the modulated temperature step-scanning mode is analogous to the $P(t)$ curve measured under the same conditions but without modulation, as would be expected when linear response conditions are fulfilled (see Fig. 8). This finding shows that, if the degree of modulation is small enough, modulated calorimetry can be used to study phase transitions without altering the transition process.

The values for ΔH_m measured at decreasing temperature scanning rates, as reported in Table 1, show that at β values lower than $1.66 \times 10^{-4}\ K\ s^{-1}$ the measured ΔH_m values are more and more greatly influenced by the low sensitivity of the calorimeter and significant errors are possible.

One unexpected finding in this study was the observation of two peaks in the melting curve of *n*-dodecane, which can be explained by the presence of two melting processes. The melting curves for *n*-dodecane reported in the literature have generally been obtained using scanning rates that are too high to detect the second peak. The detection of the second peak by our instrument could be due to the selective growth of larger and/or higher quality crystallites. With the very low scanning rate used, these crystallites had time to perfect during the course of the experimental runs, and the melting of the crystallites occurred at a higher temperature than that of the rest of the sample, thus allowing a second melting peak to emerge if the main peak was sufficiently narrow (low β values). This feature was not always reproducible (compare Fig. 4, where the second peak is absent in the curve at the same scanning rate shown in Fig. 1); its occurrence seems to be in part dependent on the sample preparation procedure (cooling rate, freezing temperature, storage time, and temperature). These observations strongly support our hypothesis that the second peak arises due to structural relaxation through re-crystallisation and annealing processes of the sample in the polycrystalline phase [9].

Another possible explanation for the existence of two peaks is the polymorphism of *n*-dodecane, but this hypothesis is not in agreement with the results reported by Espeau et al. [15]. These authors performed a systematic study of the structure and thermodynamics of various *n*-alkane molecules with a number n of C atoms ranging from 8 to 21, and reported observing polymorphism only for odd values of n and for $n > 20$. Their calorimetric measurements were executed using samples of 99.1% purity, but at a scanning rate of $\beta = 1/30\ K\ s^{-1}$, a rate much too high to resolve the second peak. Moreover, the temperature intervals at which the two solid phases should theoretically exist are practically superimposed, so that the crystallographic characterisation would be difficult. Therefore, the presence of polymorphism cannot be excluded. To gain further information on the solid phase of our molecule, a study of *n*-dodecane crystallisation is now in progress.

5. Conclusions

From this study many interesting features of *n*-dodecane melting have come to light. The melting curve is not always a single-peak curve; it sometimes shows a shoulder on the higher temperature side which can be attributed to the presence of a second peak. Two explanations of this feature are possible: (i) at very slow scanning rates the melting of a small number of crystallites, which have had time to become more and more perfect during the course of the run, occurs at

higher temperatures; or (ii) under particular conditions *n*-dodecane exhibits polymorphism, even if it has a low and even number of carbon atoms [15].

Our experimental results highlight the difficulty of determining the temperature of the melting transition, due to the effects of the instrument itself on the parameters being measured. The T_{onset} value, as obtained in Fig. 2, is practically independent of the experimental conditions, even at β values much higher than those reported in this paper [16]. It therefore would appear to be a good marker for the melting transition, even if a single temperature value is not sufficient to represent the complexity of a process which occurs over a temperature interval.

The temperature step-scanning and the adiabatic-like step-scanning modes of MASC can be used to study processes with characteristic times longer than the instrumental time. In the case of the melting process, the instrumental time becomes very long owing to the heat diffusion in the cell + sample system [10]. The modulated temperature scanning mode would appear to be particularly promising for the study of the exact nature of the phase transition and the reversibility of the processes involved [17–19]. Such studies may be further enhanced by the combined application of the adiabatic-like mode, which can measure the cell temperature relaxation time necessary for data analysis [20].

References

[1] A.R. Ubbelohde, The Molten State of Matter, Wiley, Chichester, 1978.
[2] D. Hoffman, R.L. Miller, Polymer 38 (1997) 3151.
[3] G.A. Arteca, J. Phys. Chem. B 101 (1997) 4092.
[4] B. Sirota, D.M. Singer, J. Chem. Phys. 101 (1994) 1087.
[5] G. Ungar, J. Phys. Chem. 87 (1983) 689.
[6] B. Ewen, G.R. Strobl, D. Richter, Faraday Discuss. Chem. Soc. 69 (1980) 19E.
[7] G. Salvetti, C. Ferrari, F. Papucci, E. Tombari, Italian Patent Deposit PI98A000044 (1998) and PI98A000073 (1998).
[8] B. Sirota, Langmuir 14 (1998) 3133.
[9] G.P. Johari, Philos. Mag. B77 (1998) 1367, and references therein.
[10] G. Salvetti, C. Cardelli, C. Ferrari, E. Tombari, Thermochim. Acta, in press.
[11] G. Salvetti, C. Ferrari, E. Tombari, Thermochim. Acta 316 (1998) 47.
[12] Handbook of Chemistry and Physics, 58th Edition, CRC Press, Boca Raton, FL, 1977.
[13] C. Plato, A.R. Glasgow, J. Anal. Chem. 41 (1969) 330.
[14] H.L. Finke, M.E. Gross, J. Am. Chem. Soc. 76 (1954) 333.
[15] P. Espeau, et al. J. Chim. Phys. 93 (1996) 1217.
[16] C. Schick, private communication.
[17] A. Toda, T. Oda, M. Hikosaka, Y. Saruyama, Thermochim. Acta 293 (1997) 47.
[18] C. Schick, M. Merzyiakov, M. Zorzut, A. Wurm, Europhys. Conf. Abstr. 22I (1998) 113.
[19] I. Okazaki, B. Wunderlich, Macromolecules 30 (1997) 1758.
[20] G.W.H. Höhne, Thermochim. Acta 330 (1999) 45.